ELSEVIER

Resonant helical deformations in nonhomogeneous Kirchhoff filaments

Alexandre F. da Fonseca[a], C.P. Malta[a,*], M.A.M. de Aguiar[b]

[a]*Instituto de Física, Universidade de São Paulo, USP Rua do Matão, Travessa R, Cidade Universitária, 05508-900 São Paulo, Brazil*
[b]*Instituto de Física 'Gleb Wataghin', Universidade Estadual de Campinas, UNICAMP 13083-970, Campinas, SP, Brazil*

Abstract

We study the three-dimensional static configurations of nonhomogeneous Kirchhoff filaments with periodically varying Young's modulus. We analyze the effects of the Young's modulus frequency and amplitude of variation in terms of stroboscopic maps, and in the regular (non chaotic) spatial configurations of the filaments. Our analysis shows that the tridimensional conformations of long filaments may depend critically on the Young's modulus frequency in case of resonance with other natural frequencies of the filament. As expected, far from resonance the shape of the solutions remain very close to that of the homogeneous case. In the case of biomolecules, although various other elements, besides sequence-dependent effects, combine to determine their conformation, our results show that sequence-dependent effects alone may have a significant influence on the shape of these molecules, including DNA.
© 2005 Elsevier B.V. All rights reserved.

*Corresponding author. Fax: + 55 11 3814 0503.
E-mail address: coraci@if.usp.br (C.P. Malta).

The study of tridimensional structures of filamentary objects is of great interest in several areas of knowledge, ranging from microscopic to macroscopic systems. Examples of macroscopic systems in Engineering are the stability of suboceanic cables [1,2] and installation of optical fibers [3,4]; in Biology, the shape of climbing plants [5]; and, in Physics and Mathematics, the shape and dynamics of cracking whips [6]. Microscopic examples are found in Structural Biology, as in the study of the structure of biomolecules [7,8] and bacterial fibers [9,10], and in Nanoscience, as the study of the elastic properties of nanosprings [11].

Filamentary systems are usually modeled as thin *uniform* rods. However, nonuniformities in the filament properties can affect significantly its tridimensional structure. In this work we study certain resonant variations in the shape of helical rods induced by periodic variations in the stiffness of the rod. One of the motivations for this theoretical study is, on one hand, the observation that the DNA stiffness is sequence-dependent [12]. On the other hand, it is also known [13,14] that a substantial fraction of all eukaryotic genomes are composed of tandemly repeated sequences of base-pairs. These repetitive DNAs are formed by nucleotide sequences of varying length and composition reaching up to 100 megabasepairs of length [14]. Usually they are regarded as "selfish" or "junk" DNA [15] because they seem to have little or no functional role. In fact, some studies suggest that the behavior of repetitive sequences can be, in some cases, beneficial to the organism and, in others, harmful [13,14]. It could also be related to some form of cancer [16].

In this work we consider rods with small periodic variation of the Young's modulus. Since our motivation is the repetitive sequences of DNA, the numerical calculations presented here have been performed using DNA parameters. Nevertheless, the qualitative results remain valid for general rods with periodic stiffness variation. We remark that ideal elastic rod models dot not furnish realistic solutions for the spatial structure of the DNA or other biomolecules [17]. Therefore, our results for the tridimensional configurations must be considered as general mechanical tendencies due to sequence-dependent variations of the Young's modulus, rather than exact solutions for the DNA structure. Realistic models for the DNA consider base-pair parameters, as the recent theory of sequence-dependent DNA elasticity proposed by Coleman, Olson and Swigon [18], where the elastic energy depends on a function of the six kinematical variables relating the relative orientation and displacement between successive base-pairs. Thermal fluctuations play also an important role in the structure of these molecules and, therefore, statistical mechanical approaches are more appropriate to model their spatial configurations [19–21]. Nevertheless, in order to analyze the effect of periodic nonhomogeneities in equilibrium configurations, it is sufficient to take into account thermal fluctuations just roughly. This has been done by adopting an excess of 5% of linking number [22].

A table with the Young's modulus of all 32 trinucleotide units was recently obtained in Ref. [23] that can be used as a reference for the amplitude of the variation. We analyze the effects of the frequency of these periodic modulations in the Young's modulus, in terms of dynamical stroboscopic maps and directly in the tridimensional structure of the rod. We are particularly interested in understanding

how the sequence-dependent mechanical properties of the filament can cause its shape to deviate from the well known uniform solution, namely, the helix.

Mielke and Holmes [24] demonstrated that the variation of the bending stiffness along the rod can cause spatially complex tridimensional shapes and sensitivity with respect to initial conditions. They described *infinitely* long rods as initial value problems (IVP) and used analytical techniques based on dynamical systems theory to study some specific hyperbolic fixed points related to homoclinic orbits.

It should be stressed that here we analyze a case where it is not possible to use the perturbative methods of dynamical systems theory, therefore we had to resort to numerical simulations.

The Kirchhoff rod model has been extensively used in the literature to model continuous rods [25–27]. For example, Shi and Hearst [28] and Nizette and Goriely [29] obtained and classified, respectively, all the solutions of the static Kirchhoff equations for homogeneous rods with circular cross section. Coleman et al. [30] made a complete analysis of the stability of DNA within the framework of the Kirchhoff rod model, subjected to strong anchoring end conditions. Recently, Neukirch [31] used the Kirchhoff rod model to study the twist rigidity of single supercoiled DNA molecules. Neukirch and Henderson [32,33] studied the properties of the equilibrium configurations of homogeneous rods subjected to clamped boundary conditions. Da Fonseca and de Aguiar [34] compared homogeneous and nonhomogeneous rods, with varying stiffness, subjected to boundary conditions. The effects of nonhomogeneous mass distribution in the dynamics of unstable closed rods have been analyzed by Fonseca and de Aguiar [35]. Yang et al. [8] have studied a particular case of nonhomogeneous Young's modulus for closed rods. Manning et al. [36] have incorporated into the Kirchhoff model the sequence-dependent discrete data of the intrinsic curvature of DNA. In the present study we assume that the DNA is intrinsically an untwisted straight rod, but we include sequence-dependent stiffness.

In the Kirchhoff model for an inextensible rod the Young's modulus appears in the equations through its *bending* coefficient. As there is no table with the *bending* coefficients for all *di* or *trinucleotides*, we shall consider the data in Ref. [23] as a reference for our calculations, as mentioned.

We shall consider the Hamiltonian formulation of the Kirchhoff's equations. We shall follow the simplest derivation by Nizette and Goriely [29] instead of the rigorous Hamiltonian formulation by Mielke and Holmes [24]. The reader is referred to Refs. [26,27,35] for a derivation of the Kirchhoff model, and to Ref. [29] for the Hamiltonian formulation. Hamilton's equations for the Kirchhoff model are analogous to those of a symmetric spinning top in a gravity field, with the arc length s along the rod playing the role of time. The main advantage of a Hamiltonian formulation is that the theory of chaotic Hamiltonian systems and stroboscopic maps can be directly applied to understand the spatial behavior of the filament. The length of the tandemly repeated sequences can reach up to 100 megabasepairs [14] while the length of the repeats is no more than a few hundreds of basepairs long. So we shall solve the Kirchhoff's equations as an IVP to find the conformational solutions of the filament problem.

The Hamiltonian for an elastic rod with circular cross section, in Euler angles, is

$$H = \frac{P_\theta^2}{2E} + \frac{P_\phi^2}{2\Gamma_0\mu} + \frac{(P_\psi - P_\phi \cos\theta)^2}{2E \sin^2\theta} + F \cos\theta \,. \tag{1}$$

The Euler angles θ, ϕ and ψ connect a fixed Cartesian basis $\{\mathbf{e}_1, \mathbf{e}_2, \mathbf{e}_3\}$ to the *local orthonormal basis* $\mathbf{d}_i = \mathbf{d}_i(s, t)$, $i = 1, 2, 3$, attached to each point of the rod. The direction of $\mathbf{e}_3$ is chosen to be the direction of the constant force $\mathbf{F}$. $\mathbf{d}_3$ is chosen to be tangent to the curve $\mathbf{x}(s)$ that defines the axis of the filament, and $\mathbf{d}_1$ and $\mathbf{d}_2$ are in the direction of the principal moments of inertia of the cross section (perpendicular to $\mathbf{d}_3$). The momentum P_ψ is the $\mathbf{e}_3$-component of the angular momentum with respect to the axis of the rod and P_ϕ is the torsional moment, i.e., the momentum with respect to $\mathbf{d}_3$ [29]. They remain constant along the rod even if E and μ depend on the arc length s. The Hamiltonian, Eq. (1), will depend on s through $E(s)$ and $\mu(s)$.

The parameters $E = E(s)$ and $\mu = \mu(s)$ are the scaled Young's and shear moduli, respectively. F is the intensity of the total contact force (constant) exerted on the cross section at s. The units used here are the same of Refs. [26,27,35]. Γ_0 varies between $2/3$ (incompressible material) and 1 (hyper-elastic material), and it should be remarked that Γ_0 has no influence in the equilibrium solutions. The momenta are defined by

$$\begin{aligned} P_\theta &\equiv E(s)\theta' \,, \\ P_\phi &\equiv \Gamma_0\mu(s)(\phi' + \psi' \cos\theta) \,, \\ P_\psi &\equiv E(s)\psi' \sin^2\theta + P_\phi \cos\theta \,, \end{aligned} \tag{2}$$

where the prime indicates the derivative with respect to s.

In the case of a homogeneous filament, $E(s) \equiv 1$ and $\mu(s) \equiv 1$ in Eq. (1), and the Hamiltonian is written as

$$H = \frac{P_\theta^2}{2} + \frac{P_\phi^2}{2\Gamma_0} + V(\theta) \,, \tag{3}$$

where the potential $V(\theta)$ is

$$V(\theta) = \frac{(P_\psi - P_\phi \cos\theta)^2}{2\sin^2\theta} + F \cos\theta \,. \tag{4}$$

If $P_\psi = P_\phi$, then $\theta = 0$ (straight rod) is an equilibrium solution, and if $F \neq 0$ there is a second equilibrium solution ($\theta \neq 0$) corresponding to a helix [37]. If $P_\psi = -P_\phi$, the equilibrium solution is $\theta = \pi$, and if $F \neq 0$ there is a second equilibrium solution as above. If $|P_\psi| \neq |P_\phi|$ then $V(\theta)$ (4) has a single minimum corresponding to the well known helix solution. Denoting by θ_0 the point of minimum of the potential (4), the frequency ω_0 of small oscillations around θ_0 is given by

$$\omega_0 = P_\phi^2 + 2V(\theta_0) - 6F \cos\theta_0. \tag{5}$$

In the Appendix we show that the potential $V(\theta)$ (4) cannot be well approximated by a second-order expansion in the neighborhood of its minimum (it is expanded up to order 6).

We shall consider the following periodic variation of the scaled Young's modulus

$$E(s) = 1 + \alpha \cos \omega s . \tag{6}$$

The parameter α is the amplitude of the Young's modulus periodic variation, and ω is the frequency of the oscillation. We are concerned only with the tridimensional shape of the rod and it should be stressed that the shear modulus $\mu(s)$ does not affect the tridimensional configuration.

To obtain the equilibrium configurations we first solve Hamilton's equations for θ and P_θ. Then, we solve Eq. (2) for ψ and reconstruct the filament by integrating $\mathbf{d}_3$ along s

$$\mathbf{x}(s) = \int_0^s [(\sin \theta \cos \psi)\mathbf{e}_1 + (\sin \theta \sin \psi)\mathbf{e}_2 + (\cos \theta)\mathbf{e}_3] \, ds' . \tag{7}$$

Notice that $\mathbf{x}(s)$ is a function of the initial conditions $\theta(s = 0) \equiv \theta_0$ and $P_\theta(s = 0) \equiv P_0$. Without lack of generality, P_0 can be set equal to 0 so that θ_0 will be a conformation parameter. In solving the equation for ψ we set its initial value $\psi_0 = 0$.

In what follows we present numerical calculations performed with the following fixed mechanical parameters: $\alpha = 0.1$, $P_\psi = 0.086$, $P_\phi = 0.043$ and $F = 20$ pN. These parameters, excepting the force F, are written in properly scaled units. The maximum value for α is 0.66, in accordance with the table of the DNA Young's modulus presented in Ref. [23]. The value of P_ϕ used corresponds to an excess of 5% of the linking number [22] due to thermal fluctuations. The value of the force corresponds to a compressing force consistent with the values in the literature [38].

Fig. 1 displays nine stroboscopic maps on the θ–P_θ plane for different values of frequency ω. We start with $\omega = 0.60\omega_0$ (Fig. 1a) where a larger stability island encloses the main equilibrium point at $\theta \simeq 2.08$ rad and $P_\theta = 0$, and a smaller island is seen on the left, at $\theta \simeq 0.5$ rad. The frequency goes up to $\omega = 2.00\omega_0$. We recall that spatial chaos has been observed before in the Kirchhoff equations [24,39].

As we go through the sequence of stroboscopic maps displayed in the Fig. 1, the large island in the plate (a) slowly shrinks and eventually disappears at $\omega \approx \omega_0$ (Figs. 1e and f). A second important island appears at $\omega \approx 0.82\omega_0$ (Fig. 1b). This new island increases in size and moves towards the right as ω is increased. Besides these two main islands, a number of smaller and short-lived islands pop up and disappear as ω changes, a phenomenon typical of chaotic maps. We shall concentrate our study on the two main islands described above, since they dominate the stroboscopic maps and last for large intervals of ω.

We shall now investigate the differences in the shape of the tridimensional configurations corresponding to the two equilibrium points lying at the center of these islands. In order to construct the rods we solved the Hamiltonian equations using the values of the equilibrium point for θ and P_θ as initial conditions θ_0 and P_0 and used Eq. (7) to construct the filament.

The tridimensional configuration corresponding to the equilibrium point changes as the frequency is varied. The shape evolution is displayed in Figs. 2 and 3 for the two main equilibrium points mentioned above.
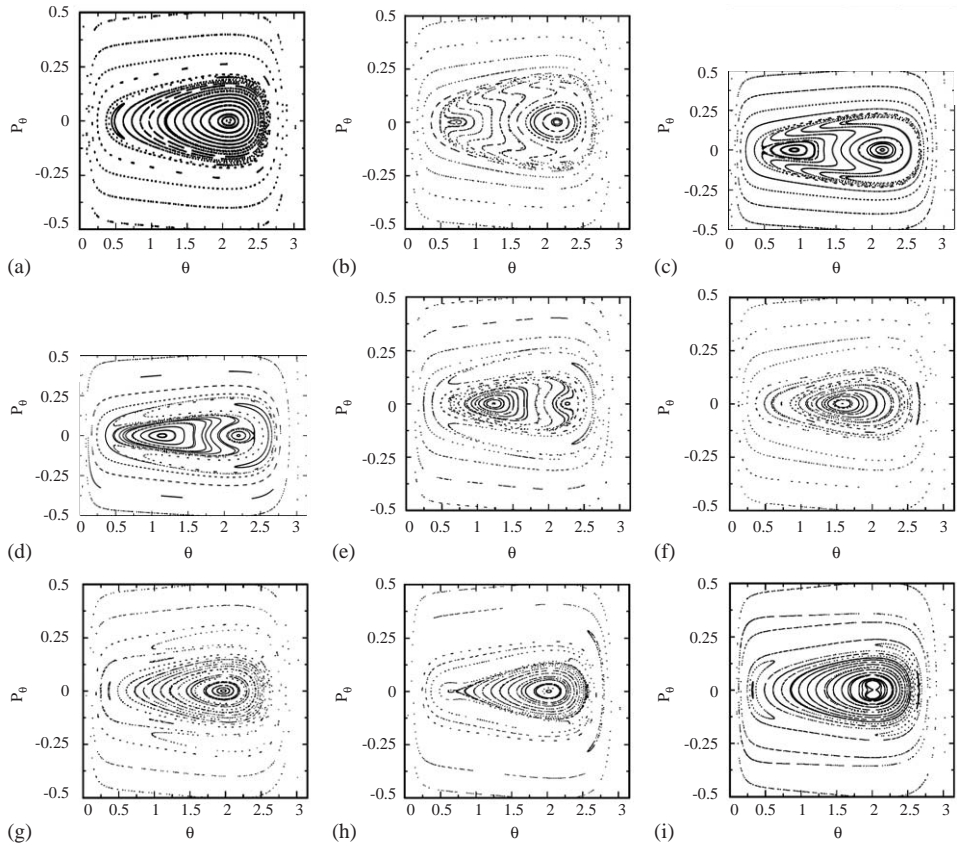
Fig. 1. Stroboscopic maps for $P_\psi = 0.086$, $P_\phi = 0.043$ and $F = 20$ pN. The frequency of the Young's modulus oscillation in each map is: (a) $\omega = 0.60\omega_0$; (b) $\omega = 0.82\omega_0$; (c) $\omega = 0.85\omega_0$; (d) $\omega = 0.90\omega_0$; (e) $\omega = 0.92\omega_0$; (f) $\omega = 1.00\omega_0$; (g) $\omega = 1.20\omega_0$; (h) $\omega = 1.60\omega_0$; (i) $\omega = 2.00\omega_0$.

In Fig. 2, panels (a)–(d), we show the shape evolution of the configuration corresponding to the first main equilibrium point which lies in the center of the main island appearing in Fig. 1a, and in the center of the island on the right in Figs. 1b, c and e, respectively. We can see that the shape of the rod deviates more and more from the helix pattern as ω is increased, becoming rather twisted for $\omega = 0.92\omega_0$.

In Fig. 3, panels (a)–(d), we show the shape evolution of the configuration corresponding to the other main equilibrium point which lies in the center of the 'left island' (born in Fig. 1b). The configurations shown in Figs. 3a–d correspond to the frequency values used in the Figs. 1b, c, f and h, respectively. The behavior of this sequence of rod shapes is the reverse of that corresponding to the first equilibrium point (Fig. 2). As ω increases, the shape becomes less coiled and eventually recovers the near-helix shape, similar to the rod in Fig. 2a, corresponding to the first equilibrium point (Fig. 1a).
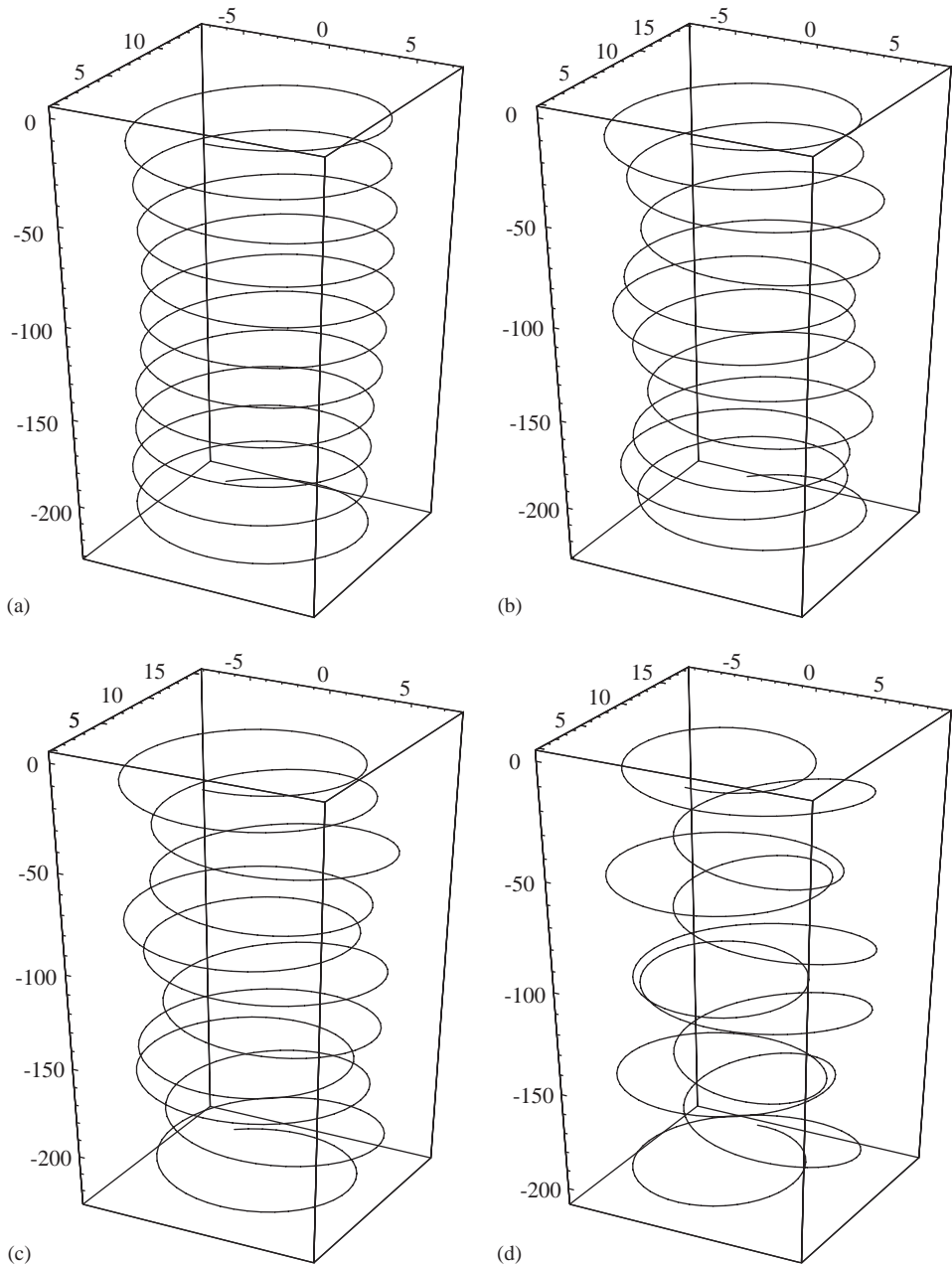
Fig. 2. Shape evolution of the conformations corresponding to the center of the main island seen in Fig. 1a. (a) $\omega = 0.60\omega_0$ (Fig. 1a); (b) $\omega = 0.82\omega_0$ (Fig. 1b); (c) $\omega = 0.85\omega_0$ (Fig. 1c); (d) $\omega = 0.92\omega_0$ (Fig. 1e).
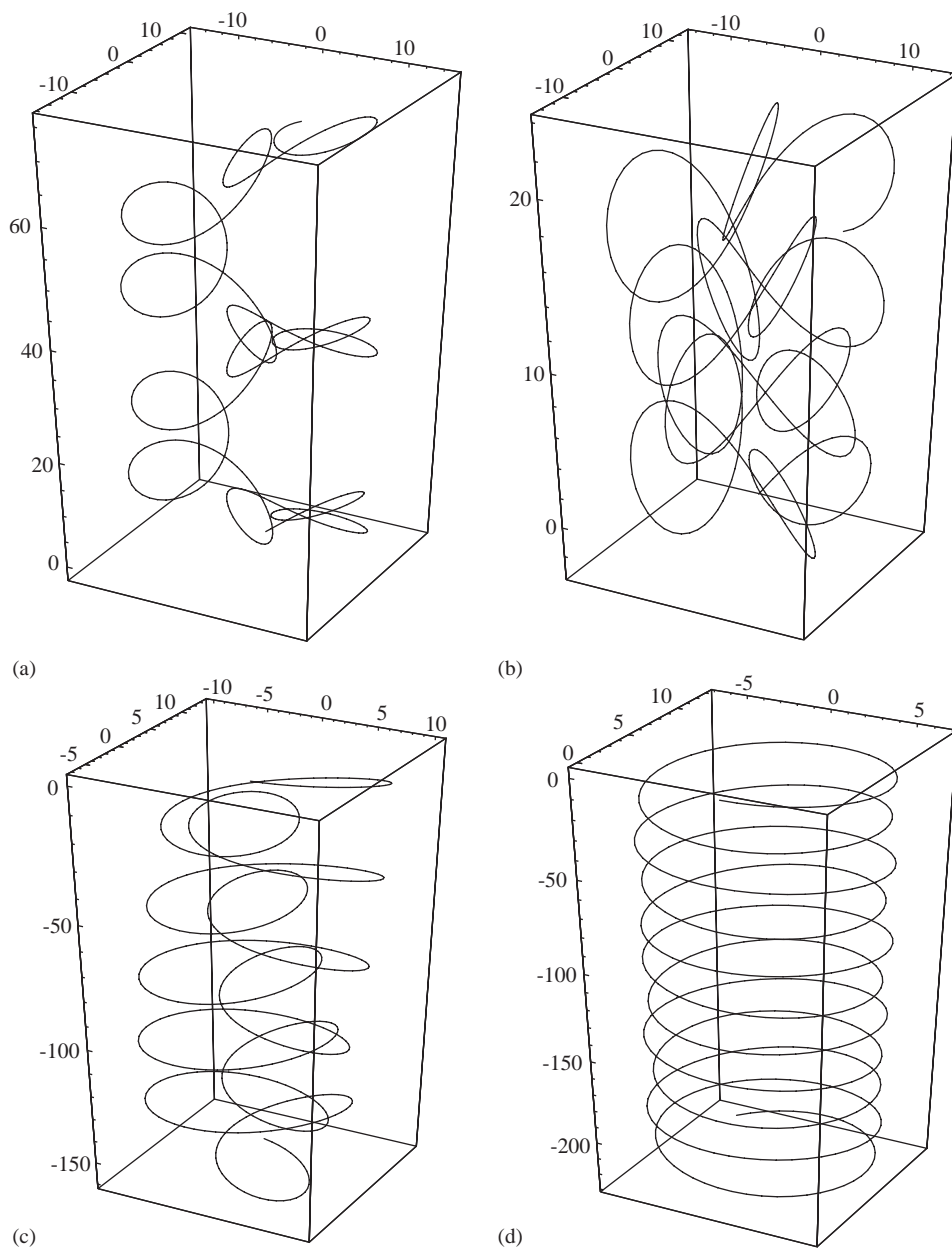
Fig. 3. Shape evolution of the conformations corresponding to the center of the left island that appears when $\omega > 0.81\omega_0$ (Fig. 1b). (a) $\omega = 0.82\omega_0$ (Fig. 1b); (b) $\omega = 0.85\omega_0$ (Fig. 1c); (c) $\omega = \omega_0$ (Fig. 1f); (d) $\omega = 1.60\omega_0$ (Fig. 1h).

Finally, when $\omega = 2\omega_0$, Fig. 1i, a period-doubling bifurcation occurs. The orbit at the center of the island becomes unstable and a new stable equilibrium, with twice the original period, appears.

The sensitivity of the shape of the nonhomogeneous rods to the amplitude of the nonhomogeneity can also be tested. Fig. 4 shows, for the same mechanical parameters of the previous figures, the helix solution of the homogeneous case (left), the solution for $\alpha = 0.001$ (middle) and the solution for $\alpha = 0.01$ (right), in the resonant case $\omega = \omega_0$. Also, these solutions can be compared to that in the Fig. 3c. We can see that even for very small values of the amplitude α, the tridimensional configuration deviates fast from the helix solution at the resonance.

It is interesting to notice that, as the frequency increases, the position of the equilibrium points move in the direction of increasing θ. Fig. 5 displays the value of θ corresponding to the equilibrium point related to the main (circles) and to the left (square) islands as function of ω. The dotted line indicates θ_0 which is the position of the equilibrium point of the potential $V(\theta)$ related to the homogeneous case. As we can see in the Figs. 2a and 3d, the shape of the corresponding tridimensional configuration becomes similar to the helix when the position of the equilibrium position gets close to θ_0 (homogeneous case equilibrium point position).

The main result of this numerical experiment is that the tridimensional conformations of long filaments may depend critically on sequence-dependent properties if these are in resonance with other natural periods of the filament. As expected, in the limit of very low or very high frequencies, as compared to ω_0, the shape of the solutions remain very close to that of the homogeneous case. In the case of biomolecules, it is well known that various other elements, besides sequence-
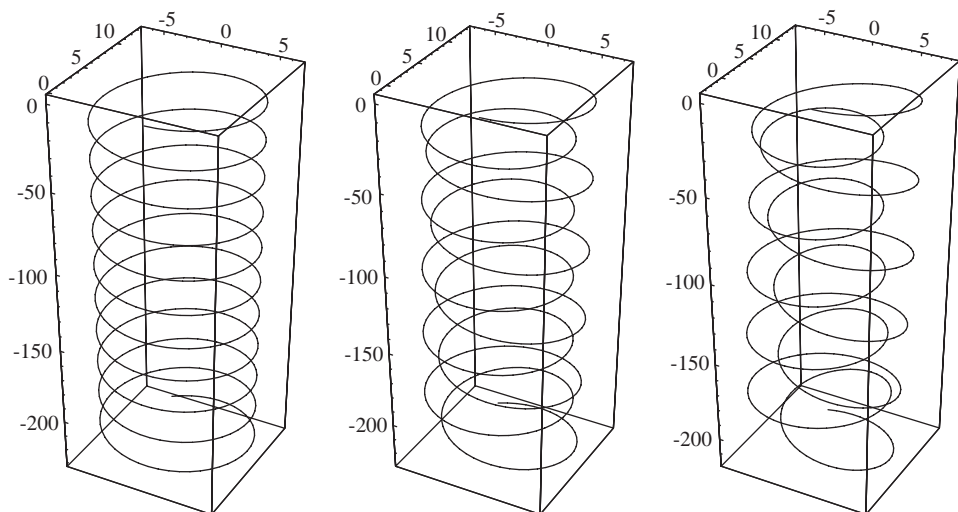

Fig. 4. Tridimensional shape of the configurations corresponding to the center island that appears in the stroboscopic maps for $\omega = \omega_0$ and different α (stroboscopic maps not shown). From left to right, homogeneous case, $\alpha = 0.001$ and 0.01.
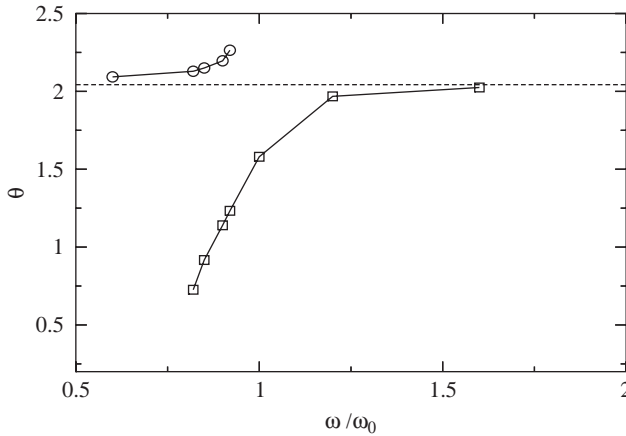
Fig. 5. Position of the equilibrium points as function of the frequency ω, circles corresponding to the center of the main island in the stroboscopic maps of Figs. 1a–e, and squares to the center of the left island that appears when $\omega > 0.81\omega_0$ (Figs. 1b–h). The dotted line corresponds to θ_0, homogeneous case equilibrium point position.

dependent effects, combine to determine their conformation, like self-contact, salt concentration, thermal fluctuations, anisotropy and interaction with proteins. Our results show that sequence-dependent effects alone may have a significant influence on the shape of these molecules, including DNA.

Appendix A

Here we show that the potential $V(\theta)$ of Eq. (4) cannot be well approximated by an expansion up to order 2 or 3 around its minimum at ($\theta = \theta_0$). This is due to the presence of $\sin^2 \theta$ in the denominator of one of the terms of the $V(\theta)$. To illustrate this, we expand $V(\theta)$, up to order 6 in ($\theta - \theta_0$), for the same numerical parameters used in this paper,

$$V(\theta) = V(\theta_0) + 0.0205(\theta - \theta_0)^2 + 0.0227(\theta - \theta_0)^3 + 0.0235(\theta - \theta_0)^4$$
$$+ 0.0257(\theta - \theta_0)^5 + 0.0275(\theta - \theta_0)^6 + O[(\theta - \theta_0)^7], \qquad (A.1)$$

where $\theta_0 \simeq 2.043$ for this case.

Since the coefficients of the terms $(\theta - \theta_0)^n$ have the same order of magnitude, it is necessary to check if $(\theta - \theta_0) \ll 1$ for all $\theta(s)$, i.e., along the rod. We found that for the frequency ω of the Young's modulus far from the resonance ($|\omega - \omega_0| \gg 0$), the solutions corresponding to the equilibrium points have $(\theta(s) - \theta_0)_{MAX} \simeq 0.03$, where the subscript MAX means "maximum value for all s". But at the resonance, $\omega = \omega_0$,

the solution corresponding to the equilibrium point has $(\theta(s) - \theta_0)_{\mathrm{MAX}} \simeq 0.5$. $(\theta(s) - \theta_0)_{\mathrm{MAX}}$ becomes even larger than 0.5 if we consider the solution related to the new equilibrium point (the new island that appeared in the map displayed in Fig. 1b).

Therefore, the perturbative method of the dynamical systems theory is not applicable to analyzing this case.

References

[1] J. Coyne, IEEE J. Ocean. Eng. 15 (1990) 72.
[2] E.E. Zajac, J. Appl. Mech. 29 (1962) 136.
[3] Y. Sun, J.W. Leonard, Ocean. Eng. 25 (1997) 443.
[4] M.A. Vaz, M.H. Patel, Appl. Ocean Res. 22 (2000) 45.
[5] A. Goriely, M. Tabor, Phys. Rev. Lett. 80 (1998) 1564.
[6] A. Goriely, T. McMillen, Phys. Rev. Lett. 88 (2002) 244301.
[7] T. Schlick, Curr. Opin. Struct. Biol. 5 (1995) 245;
    W.K. Olson, Curr. Opin. Struct. Biol. 6 (1996) 242.
[8] Y. Yang, I. Tobias, W.K. Olson, J. Chem. Phys. 98 (1993) 1673.
[9] C.W. Wolgemuth, T.R. Powers, R.E. Goldstein, Phys. Rev. Lett. 84 (2000) 1623.
[10] I. Klapper, J. Comput. Phys. 125 (1996) 325.
[11] A.F. da Fonseca, D.S. Galvão, Phys. Rev. Lett. 92 (2004) 175502.
[12] W.K. Olson, A.A. Gorin, X.-J. Lu, L.M. Hock, V.B. Zhurkin, Proc. Natl. Acad. Sci. USA 95 (1998) 11163.
[13] J. Hsieh, A. Fire, Annu. Rev. Genet. 34 (2000) 187.
[14] B. Charlesworth, P. Sniegowski, W. Stephan, Nature 371 (1994) 215.
[15] B.F. McAllister, J.H. Werren, J. Mol. Evol. 48 (1999) 469.
[16] G. Aquilina, M. Bignami, J. Cell. Physiol. 187 (2001) 145.
[17] W.K. Olson, V.B. Zhurkin, Curr. Opin. Struct. Biol. 10 (2000) 286.
[18] B.D. Coleman, W.K. Olson, D. Swigon, J. Chem. Phys. 118 (2003) 7127.
[19] C. Bouchiat, M. Mézard, Phys. Rev. Lett. 80 (1998) 1556.
[20] C. Anselmi, G. Bocchinfuso, P. De Santis, M. Savino, A. Scipioni, Biophys. J. 79 (2000) 601.
[21] S. Panyukov, Y. Rabin, Phys. Rev. Lett. 85 (2000) 2404.
[22] J.F. Marko, E.D. Siggia, Phys. Rev. E 52 (1995) 2912.
[23] M.M. Gromiha, J. Biol. Phys. 26 (2000) 43.
[24] A. Mielke, P. Holmes, Arch. Rational Mech. Anal. 101 (1988) 319.
[25] G. Kirchhoff, J. Reine Angew. Math. 56 (1859) 285.
[26] E.H. Dill, Arch. Hist. Exact. Sci. 44 (1992) 2;
    B.D. Coleman, E.H. Dill, M. Lembo, Z. Lu, I. Tobias, Arch. Rational Mech. Anal. 121 (1993) 339.
[27] A. Goriely, M. Tabor, Phys. Rev. Lett. 77 (1996) 3537;
    A. Goriely, M. Tabor, Physica D 105 (1997) 20.
[28] Y.M. Shi, J.E. Hearst, J. Chem. Phys. 101 (1994) 5186.
[29] M. Nizette, A. Goriely, J. Math. Phys. 40 (1999) 2830.
[30] I. Tobias, D. Swigon, B.D. Coleman, Phys. Rev. E 61 (2000) 747;
    B.D. Coleman, D. Swigon, I. Tobias, Phys. Rev. E 61 (2000) 759.
[31] S. Neukirch, Phys. Rev. Lett. 93 (2004) 198107.
[32] S. Neukirch, M.E. Henderson, J. Elasticity 68 (2002) 95.
[33] M.E. Henderson, S. Neukirch, Int. J. Bifurcation Chaos 14 (2004) 1223.
[34] A.F. da Fonseca, M.A.M. de Aguiar, Physica D 181 (2003) 53.
[35] A.F. Fonseca, M.A.M. de Aguiar, Phys. Rev. E 63 (2001) 016611.
[36] R.S. Manning, J.H. Maddocks, J.D. Kahn, J. Chem. Phys. 105 (1996) 5626.
[37] G.H.M. van der Heijden, J.M.T. Thompson, Nonlinear Dyn. 21 (2000) 71.
[38] R.B. Macgregor Jr., Biopolymers 48 (1998) 253;
    V. Norris, T. Onoda, H. Pollaert, G. Grehan, BioSystems 49 (1999) 71.
[39] M.A. Davies, F.C. Moon, Chaos 3 (1993) 93.